SELF-AFFINE TWO DIMENSIONAL INTERMITTENCY IN ^{28}Si–Ag/Br INTERACTION AT 14.5A GeV

Provash Mali, Amitabha Mukhopadhyay

Department of Physics, University of North Bengal
Darjeeling 734013, West Bengal, India

Gurmukh Singh

Department of Computer and Information Science
SUNY at Fredonia, Fredonia, New York 14063, USA

(Received October 18, 2011; revised version received January 20, 2012; final version received February 2, 2012)

The density fluctuation of the final state charged mesons are investigated in terms of two-dimensional scaled factorial moments in ^{28}Si–Ag/Br interaction at an incident energy of 14.5 GeV per nucleon. The experimental results are compared with a microscopic transport model based on the Ultra-relativistic Quantum Molecular Dynamics (UrQMD). To accommodate the Bose–Einstein type correlation, that dominates the origin of intermittency, an algorithm based on reassigning charges of produced particles has been employed to the UrQMD data. However, our investigation shows that a strong self-affine intermittent behavior in the experiment still cannot be replicated by the simulation. The Hurst exponent is used to account for the experimentally observed anisotropy in the pseudorapidity — azimuthal angle plane. The usual power law type of scaling behavior of the factorial moments, typical of intermittency in one dimension, is retrieved only when independent phase-space directions are partitioned unequally. Several issues related to the underlying (multi)fractal structure of the density function are also examined.

DOI:10.5506/APhysPolB.43.463
PACS numbers: 25.75.–q, 25.70.Mn, 24.60.Ky

1. Introduction

In order to study the non-statistical (dynamical) fluctuation of the single particle density distribution in the final state of any high-energy interaction, a technique based on the scaled factorial moment (SFM) measurement was

first introduced by Bialas and Peschanski [1,2]. The SFM F_q of the order of q (a positive integer) defined for the phase space partition number M, and appropriately normalized by the mth bin (phase space interval) multiplicity n_m is given by

$$F_q = \frac{1}{M}\sum_{m=1}^{M}\frac{\langle n_m(n_m-1)\dots(n_m-q+1)\rangle}{\langle n_m\rangle^q}\,. \tag{1}$$

The entire phase-space interval ΔX over which the analysis is made, is divided into equal size subintervals $\delta X\,(=\Delta X/M)$, and the brackets $\langle\rangle$ on the right-hand side of the above expression denote averaging over many events which is done for statistical reasons. If the fluctuations under consideration are self-similar at all scales, F_q is expected to increase with decreasing δX following a power law

$$F_q \sim (\delta X)^{-\phi_q}\,, \qquad \delta X \to 0\,. \tag{2}$$

In multiparticle production physics the phenomenon is known as 'intermittency', where ϕ_q is a scale invariant positive definite quantity called the intermittency exponent (index). Several speculative measures, some conventional and a few other exotic, are adopted to interpret the intermittency results in high-energy interactions. As for example, the intermittency phenomenon can be explained in terms of the ordinary BE type of correlation [3,4], arising out of an enhanced yield in the like charge sign mesons within narrow phase-space intervals. While incorporating the BE correlation (BEC) into numerical modeling certainly reduces the mismatch between the observation and the Monte Carlo (MC) simulation [5], the experimental results cannot always be fully accounted for. Large particle densities within narrow phase-space region may also occur due to collective effects [6,7] like the Cherenkov gluon emission [8]. The intermittency may as well be due to a QCD parton shower cascading process of particle emission [9], or it may even be due to a non-thermal phase transition [10] similar to that observed in the spin glass system. Last but not least, large fluctuations in the final state particle density particularly in nucleus–nucleus (AB) collisions, may be an outcome of a transition from the exotic quark-gluon plasma (QGP) to the ordinary hadronic phase [11,12]. The picture till date is neither complete nor very clear. There still exist plenty of unresolved issues related to this phenomenon that need to be further scrutinized.

The existence of dynamical components in particle density fluctuations has been confirmed in many high energy interactions. There are some excellent compilations on the recent progress of the subject (see reviews [13,14]). Many of the intermittency analyses mentioned in [13,14] were performed in one dimension (1d), mostly in the rapidity (y) or in the pseudorapidity

(η) space. The actual process of particle production however, takes place in three dimension. When the dynamics is projected onto a lower dimension, the effects of fluctuation are reduced or they can even be completely washed out [9]. In high-energy collisions it is observed that the heavier is the colliding system or the more is the collision energy, the weaker is the intermittency in (1d). On the other hand, in higher dimensions not only the intermittency grows in its strength, but one also finds an upward bending in the log–log variation of the SFM with increasing phase-space resolution [15,16], both of which in contrast to the (1d) case, are stronger in heavier colliding systems.

Very recently, we have performed a (1d) analysis of a set of ^{28}Si–Ag/Br data at an incident energy of 14.5A GeV [17], where the experimental measurements are compared with a set of simulated data based on the UrQMD code [18]. We observed that the experimental intermittency strength in the azimuthal (φ) space is approximately twice as large as that in the η-space, while the UrQMD model produces negligible intermittency in both spaces. There are indications of non-thermal phase transition as well as random cascading during the particle production process. In this paper we are going to extend our analysis to the two-dimensional (2d) intermittency of the same set of data on ^{28}Si–Ag/Br interaction. The main motivations are *(i)* to investigate the anisotropy in the (2d) particle density in the (η, φ) plane in terms of self-affine (multi)fractal structure, and *(ii)* to check whether or not the BEC, implemented in the UrQMD code at the level of the so-called after-burner, can account for the experiment. The BE type of correlation is accommodated into the UrQMD data by employing an algorithm [19,20], that reassigns the charges of produced pions but does not alter their original four-momenta or the space time coordinates as given by the event generator. The paper is organized in the following way. In Section 2 the experimental data collection method, and in Section 3 the simulated data generation method are briefly discussed. In Section 4 we describe the statistical technique(s) employed to analyze the data and the results obtained from the analysis. In Section 5 we conclude with a summary of our observations and incorporate a few critical remarks on the same. Whenever necessary, we shall refer back to our previous intermittency related works on AB interactions [21,22,23].

2. Experiment

Ilford G5 nuclear emulsion pellicles of size $16\,\text{cm} \times 10\,\text{cm} \times 600\,\mu\text{m}$, irradiated by the ^{28}Si beam obtained from the Alternating Gradient Synchrotron at the Brookhaven National Laboratory (USA) were used to collect the data. The incident beam energy was 14.5 GeV per nucleon. To find out the primary ^{28}Si–Ag/Br events the emulsion plates were scanned along individual projectile tracks with Leitz microscopes under a total magnification 300×.

Angle measurement and track counting/classification were performed under a total magnification 1500× by using a pair of Koristka microscopes. Minute details of nuclear emulsion technique are thoroughly discussed in [24,25]. In emulsion terminology tracks emerging from an interaction vertex are classified in the following way.

(i) Shower tracks: The shower tracks are caused by the singly charged particles produced in an interaction (also called a star), and moving with a very high speed ($v > 0.7\,c$). The ionization of this class of particles $I \leq 1.4\,I_0$, I_0 being the minimum ionization due to any particle in the emulsion pellicle, which in the present case is ≈ 20 grains/$100\,\mu$m. Mostly charged pions (contaminated by a small percentage of other mesons and e^+/e^-) belong to the shower particle category. Total number of such tracks in a single event is denoted by n_{s}.

(ii) Grey tracks: The grey tracks are caused mainly by the target recoil fast protons with ionization $1.4\,I_0 \leq I < 10\,I_0$. Their velocity values range from $0.3\,c$ to $0.7\,c$ and their kinetic energies can move up to 400 MeV. Total number of grey tracks in an event is denoted by n_{g}.

(iii) Black tracks: The black tracks are due to the heavy and slow moving fragments evaporating out of the remnants of target nuclei, having ionization $I > 10\,I_0$, velocity less than $0.3\,c$ and energy less than 30 MeV. Total number of tracks of this kind in an event is denoted by n_{b}.

(iv) Projectile fragments: The projectile fragments are nothing but the spectator parts of the incident nucleus that do not directly participate in an interaction. They are emitted within a very narrow and extremely forward cone of semi-vertex angle $\theta_{\mathrm{f}} = 0.21/p_{\mathrm{inc}}$, where p_{inc} is the incident projectile momentum per nucleons in GeV/c. The projectile fragments exhibit uniform ionization over a long range and have almost the same energy per nucleon as the beam. Their number in an event is denoted by n_{pf}.

To ensure that an event is due to an Ag/Br target nucleus only those stars were considered for which the number of heavy fragments $n_{\mathrm{h}}(= n_{\mathrm{g}} + n_{\mathrm{b}}) > 8$, while the present analysis is confined only to the produced charged particles (*i.e.*, the shower tracks). The number of ^{28}Si–Ag/Br events present in the data sample is $N_{\mathrm{ev}} = 311$ with an average shower track multiplicity $\langle n_{\mathrm{s}} \rangle = 52.67 \pm 1.33$. In emulsion experiments, η together with the azimuthal angle (φ) of a track constitutes a very convenient pair of basic variables. In the present analysis the (2d) phase space is spanned by (η, φ). For light mesons moving at relativistic speed η is an approximation of the dimensionless boost parameter y, and it is defined as

$$\eta = -\ln \tan(\theta/2)\,,$$

where θ is the emission angle of the particle/track concerned. The nuclear emulsion plates have 4π acceptance, and an accuracy of $\delta\eta = 0.1$ unit in η and $\delta\varphi = 1\,\text{mrad}$ in φ could be achieved through the reference primary method of angle measurement. Taking all 331 events together, the overall η-distribution can be approximated by a Gaussian function for which the fit parameters are, the centroid $\eta_0 = 1.90 \pm 0.01$, the width $\sigma_\eta = 2.17 \pm 0.03$ and the peak density $\rho_0 = 17.88 \pm 0.76$. On the other hand, the φ-distribution is almost uniform between 0 and 2π.

3. Simulation

Using the UrQMD code we have simulated a sample of ^{28}Si–Ag/Br interactions at 14.5A GeV that is five times as large as the experimental one. Events with Ag and Br nuclei are first generated separately, and they are thereafter mixed with each other according to the proportional abundance of Ag and Br nuclei in nuclear emulsion. All newly produced charged mesons in the simulated events are retained for subsequent analyses. The simulated event sample possesses identical multiplicity distribution, and similar η, φ-distributions as the experiment. Obviously, the average charged meson multiplicity $\langle n_{\text{ch}} \rangle$ of the UrQMD generated sample is the same as the experimental $\langle n_{\text{s}} \rangle$ quoted above. The centroid of the best Gaussian fitted η-distribution ($\eta_0 = 1.75$), and the width of the η-distribution ($\sigma_\eta = 2.15$) are also close to the respective experimental values. For error calculation *etc.* we have generated another set of event samples based on the random numbers. A pair of random numbers representing the η and φ values has been associated with each track. A linear congruential iterative method, and an inverse of integral method have been used to generate these random numbers [26]. The number of such generated event samples, each of the same size as the experimental one, in the present case is ten. Each simulated sample possesses identical multiplicity distribution, similar η-distribution (actually the best Gaussian fitted distribution), and similar φ-distribution (uniform) as the experimental sample. While generating the random numbers, no correlation has been assumed, and hence these data sets correspond to independent emission of particles. The UrQMD generated results on basic (2d) intermittency analysis are compared to the experiment.

It is known that the BE type of identical particle effect dominates the origin of intermittency. Due to correlated emission of like sign and/or opposite sign charged produced particles (mesons), the particle yield with small relative momenta is enhanced, which is one of the reasons for density fluctuation in the final state of any high-energy hadronic or nucleus induced interaction. The effect is quantum statistical in nature and it cannot be simulated by a transport model like the UrQMD. Recently, a new algorithm has been de-

veloped [19,20], where the BEC is introduced by reassigning the charges of produced mesons in such a way that the overall four-momentum distribution remains unaltered, the event wise charge multiplicities are maintained, and the particles (mesons) look like that they are satisfying the Bose statistics.

Without claiming any originality, the method of numerically modeling the BEC by using the output of the UrQMD code is very briefly described below. The UrQMD code provides the four-coordinates and the four-momenta of all particles. The particle information is contained in an ASCII file written in the OSCAR format. Each particle entry in an event contains a serial number, the particle ID, the particle four momentum (p_x, p_y, p_z, E), the particle mass m, and the final freeze-out four coordinates (x, y, z, t). In the first step we randomly choose a pion from an event, and assign a charge 'sign' *i.e.*, $+ve$, $-ve$ or 0, irrespective of its original charge with weight factors, respectively given by $p_+ = n_+/n$, $p_- = n_-/n$ and $p_0 = n_0/n$. Here n_+, n_-, n_0 are respectively, the number of $+ve$, $-ve$ and neutral pions in the event, and $n\,(= n_+ + n_- + n_0)$ is obviously the total number of pions in that event. This pion, say the ith one, defines a new phase space cell. In the next step, the distances in four-momenta $\delta_{ij}(p) = |p_i - p_j|$ and four coordinates $\delta_{ij}(x) = |x_i - x_j|$ between the already chosen pion (*i.e.*, ith) and all other pions (say the jth) that are not yet assigned any 'sign', are calculated. To each jth particle we now assign a weight factor [19]

$$P_{ij} = \exp\left[-\tfrac{1}{2}\,\delta_{ij}^2(x)\,\delta_{ij}^2(p)\right]\,, \tag{3}$$

that characterizes the bunching probability of the particles in a given cell. Then, we start generating uniformly distributed random numbers $r \in (0, 1)$. If $r < P_{ij}$ we reassign to the jth pion the same charge 'sign' as the ith one. We continue the process until r exceeds P_{ij}, or all pions in the event having the same charge 'sign' as the ith pion are exhausted. Now we go back to our first step and again randomly choose a pion from the pool for which the charge reassignment has not yet been done. Obviously, the weight factors will now be modified. The algorithm is then repeated until pions belonging to all charge varieties in the event are used up. Only pion pairs with space-like separations are accepted, and appropriate checks are made so that P_{ij} does not exceed unity [27]. Without changing the overall set of four-momenta, the four-coordinates, or the total pion charge of the system, we can in this way generate clusters of closely spaced identical charge states of pions.

4. Methodology and results

In our (2d) intermittency analysis the phase-space is the (η, φ) plane. To ensure that the SFM measurement is in no way affected by the shape of the underlying distribution(s), we first convert each of these phase-space

variables to the respective cumulant variable (X) defined as [28],

$$X_x = \int_{x_{\min}}^{x} \rho(x)dx \Big/ \int_{x_{\min}}^{x_{\max}} \rho(x)dx\,. \tag{4}$$

Here $x\,(\equiv \eta,\, \varphi)$ is the original variable, $x_{\min}(x_{\max})$ is the minimum (maximum) value of x and $\rho(x) = N_{\rm ev}^{-1}\,(dn/dx)$ is the single particle density in terms of x. Irrespective of the original variable from which it is derived, not only the particles are uniformly distributed in X_x within a range [0, 1], but the corresponding factorial moment distribution too exhibits similar translational invariance. Our $(\eta,\, \varphi)$ plane is therefore, now converted to a $(X_\eta,\, X_\varphi)$ square of unit area. We shall however, continue to call it the $(\eta,\, \varphi)$ plane. Setting the partition numbers along each direction equal *i.e.*, $M_\eta = M_\varphi$ say, this square is first symmetrically (or self-similarly) partitioned to result in $M\,(= M_\eta^2)$ smaller squares of equal size. The qth order (2d) SFM $F_q^{(2)}$ is now defined in more or less a similar way as in Eq. (1). Note that n_m is now the multiplicity in the mth sub-cell (a smaller square) of size $(\delta X_\eta \times \delta X_\varphi)$, while M is the total number of such sub-cells in the $(\eta,\, \varphi)$ plane. To begin with, we evaluate the (2d) SFMs of the order of $q = 2,\, 3$ and 4 for such equal partitioning. Fig. 1 shows the plot of $\ln F_q^{(2)}$ against $\ln M$ (which we shall later refer to as the SFM plot), (a) for the experiment, (b) for the UrQMD simulation, and (c) for the UrQMD data modified by the BEC. As mentioned before, the experimental points show a non-linear dependence of $\ln F_q^{(2)}$ on $\ln M$. In contrast, the UrQMD simulated SFMs are almost independent of M; for $q > 2$ only at large M they exhibit a irregularly

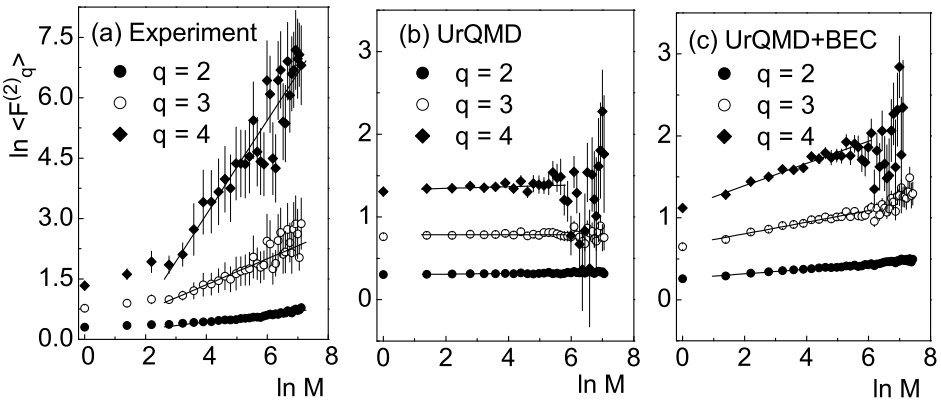

Fig. 1. Plot of $\ln\langle F_q^{(2)}\rangle$ *versus* $\ln M$ for $q = 2, 3$ and 4 for a self-similar partitioning of the $(\eta,\, \varphi)$ plane; (a) experiment, (b) UrQMD and (c) UrQMD with Bose–Einstein correlation. The lines represent linear regressions to the data points.

fluctuating pattern. On the other hand, the UrQMD data modified by the charge reassigning BEC algorithm (UrQMD+BEC), exhibit a self-similar power law of the SFM. Corresponding exponents β_q are calculated by fitting a power law type of relation like Eq. (2) to the data points. For a nonlinear variation obviously the slope will depend on the region of fit. Hence we have done it in a region, where the variations are visibly linear. The β_q values along with the χ^2 values showing the goodness of linear fit in each case, and the number of degrees of freedom (d.o.f.), are given in Table I. However, we insist that the β_q values only represent a qualitative estimate of the rise in SFM with diminishing phase space partition size. When the rise is nonlinear, these indices are in no way connected to the power law scaling, or for that matter to intermittency. On the other hand, the UrQMD generated graphs are always almost uniformly distributed showing very little or no intermittency. Correlation of any type, either due to the symmetry property of the underlying field(s) and/or due to any dynamical reason, is virtually nonexisting. When the BEC is numerically modeled into the UrQMD data, $\ln F_q^{(2)}$ shows linear rise with increasing $\ln M$ and, to some extent, we can retrieve the power law type of scaling. Corresponding β_q values also indicate that by accommodating the BEC into the simulated data, one can, to a certain degree, account for the intermittent behavior. However, as mentioned above, the experimental values are still several times larger than the (UrQMD+BEC) values, and the experiment still cannot be fully accounted for. We have also checked that in the (UrQMD+BEC) case there is hardly any non-linearity in the variation of $\ln F_q^{(2)}$ with $\ln M$. As the simulated data do not exhibit any anisotropy in the (η, φ) plane, subsequently we did not extend our self-affine analysis to the (UrQMD+BEC) case. We should mention that all experimental β_q values are also several times larger than the intermittency indices (ϕ_q) obtained in the (1d) analysis of the same set of data [17].

TABLE I

The (2d) intermittency exponents β_q of order $q = 2,\ 3$ and 4 for symmetric partitioning *i.e.*, $M_\eta = M_\varphi$.

Order	Experiment		UrQMD		UrQMD+BEC	
	β_q	χ^2 (d.o.f.)	β_q	χ^2 (d.o.f.)	β_q	χ^2 (d.o.f.)
$q = 2$	0.086±0.005	18.92(32)	0.0043±0.0027	04.27(14)	0.028±0.002	04.38(16)
$q = 3$	0.322±0.036	28.98(32)	0.0002±0.0046	10.28(14)	0.067±0.003	16.35(16)
$q = 4$	1.124±0.074	44.88(32)	0.0103±0.0092	26.45(14)	0.122±0.006	34.04(16)

It has been argued [29] that the phase-space density of multiparticle production is anisotropic, and the upward bending in the SFM plot is a direct consequence of this anisotropy. As, for example, depending on the kinematic conditions the longitudinal momenta of produced particles can vary over a wide range, whereas the average transverse momenta of these particles, irrespective of the nature of the interaction and for a reason that is still unknown to us, are limited within a relatively small range of 0.3–0.5 GeV/c. As a result, an equal bin partitioning of the (2d) distribution results in an upward bending in the corresponding SFM plot. It is suggested that in the (2d) SFM analysis the phase-space should be partitioned asymmetrically (or self-affinely as said in the fractal theory), taking the anisotropy of the phase-space into account [30]. This is done by introducing a 'roughness' parameter called the Hurst exponent (H). The anomalous scaling of the SFM that characterizes intermittency can be recovered only with a proper choice of the H value. Under such a situation the phase-space scale factors in the longitudinal (η) and the transverse (φ) directions are related as

$$\begin{aligned} M_\eta &= M_\phi^H\,, \quad \text{for} \quad H \le 1.0\,, \quad M_\phi = 1, 2, \ldots, 50\,, \\ M_\phi &= M_\eta^{1/H}\,, \quad \text{for} \quad H > 1\,, \quad M_\eta = 1, 2, \ldots, 50\,. \end{aligned} \tag{5}$$

For $H < 1.0$ the φ-direction is partitioned into finer intervals than the η-direction, whereas for $H > 1.0$ the reverse is true. It is obvious that, both M_η and M_φ simultaneously cannot always be integers. After dividing the η (φ) direction by a non-integer partition number, only the integer part is retained. As for example, if

$$\delta X_i = \Delta X_i / M_i \quad \text{and} \quad M_i = N_i + a_i \;: \qquad i = \eta \text{ or } \varphi\,, \tag{6}$$

where N_i is integer and a_i is a positive fraction (< 1) that one can do away with. In effect, contribution from a smaller strip of width $a_i \Delta X_i / M_i$ is discarded from the summation (or averaging) over bins of the factorial moment, which is done either by placing it at the beginning or at the end of all other equal sized strips of width δX_i. In doing so, no error should in principle be incurred, as the translational invariance of both the particle density and the SFM distribution have already been ensured by choosing the cumulant variables.

We have calculated $F_2^{(2)}$ as a function of M over a wide range of H (= 0.4–3.0) values. Some of them are graphically represented in Fig. 2. Once again the errors associated with the data points are statistical in origin. The solid curves in each case represent a quadratic function like

$$f(\zeta) = a\zeta^2 + b\zeta + c\,, \tag{7}$$

where $\zeta \equiv \ln M$ and $f(\zeta) \equiv \ln F_2^{(2)}$. The first two points are always excluded from the fitting process. By doing so one can get rid of the effects arising out of kinematic constraints. As for example, to conserve momentum the emitted particles tend to move in opposite directions in the φ-space, which in effect reduces the fluctuation and consequently lowers the factorial moments value. From Fig. 2 it can be seen that the strong upward bending of $\ln M$ *versus* $\ln\langle F_2^{(2)}\rangle$ plot, as it is observed for $H = 1$ in Fig. 2 (a), gets systematically weakened as H deviates from unity. For $H < 1$ we find the weakest bending at $H = 0.5$ and for $H > 1$ at 2.5. The SFM plots corresponding to these values of H are almost linear as demanded by the theory of intermittency. A quantitative description of the above observation is provided by the quadratic fit of the experimental data points in terms of Eq. (6) along with the χ^2(d.o.f.) values listed in Table II. We see that for the $H \leq 1.0$ category 'a' is minimum and 'b' is maximum at $H = 0.5$, while for the $H > 1.0$ category similar values are obtained at $H = 2.5$. The fit quality as seen from the χ^2(d.o.f.) values are always reasonably good. Our observation shows that the power law scaling of the SFM can be recovered through an asymmetric partition of the (η, φ) space.

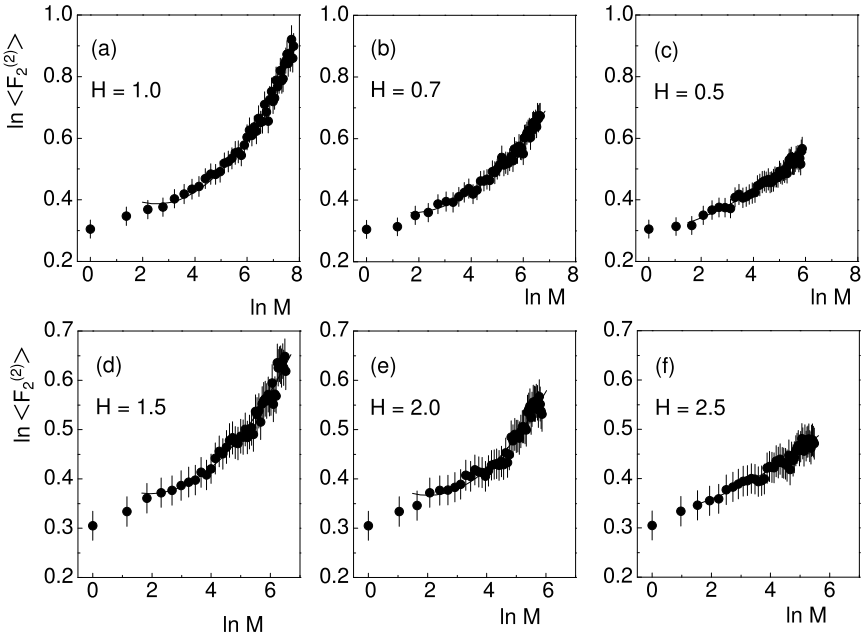

Fig. 2. Plot of $\ln\langle F_2^{(2)}\rangle$ *versus* $\ln M$ for different values of the Hurst exponent H. The lines represent best fitted quadratic function *i.e.*, $f(\xi) = a\xi^2 + b\xi + c$. First two points are excluded while fitting the function.

TABLE II

The quadratic fit parameters of Eq. (6) along with the χ^2 (d.o.f.) for different H values.

H	a	b	c	χ^2(d.o.f.)
0.4	0.0051±0.0033	0.0098±0.0321	0.0298±0.0579	6.17(45)
0.5	0.0047±0.0026	0.0155±0.0300	0.2919±0.0584	4.79(45)
0.6	0.0066±0.0032	0.0062±0.0281	0.2988±0.0581	5.72(45)
0.7	0.0121±0.0030	-0.0393±0.0274	0.3904±0.0598	6.68(45)
0.8	0.0140±0.0027	-0.0530±0.0262	0.4154±0.0602	8.57(45)
0.9	0.0145±0.0025	-0.0562±0.0252	0.4202±0.0608	8.27(45)
1.0	0.0180±0.0023	-0.0918±0.0242	0.5036±0.0615	13.5(45)
1.2	0.0152±0.0026	-0.0675±0.0258	0.4523±0.0605	7.36(45)
1.5	0.0126±0.0030	-0.0492±0.0275	0.4123±0.0591	8.45(45)
2.0	0.0132±0.0036	-0.0533±0.0295	0.4205±0.0575	8.56(45)
2.4	0.0051±0.0039	-0.0019±0.0308	0.3427±0.0570	5.18(45)
2.5	0.0032±0.0021	0.0104±0.0310	0.3246±0.0568	3.60(45)
2.6	0.0041±0.0035	0.0053±0.0313	0.3303±0.0567	3.69(45)
3.0	0.0057±0.0044	-0.0064±0.0325	0.3485±0.0566	5.49(45)

The self-affine analyses of the NA22 [31] data on pp interaction and of the NA27 [32] data on hp interactions show that the power law characterizing intermittency is obtained for $H < 1.0$, which suggests that the transverse direction has to be partitioned finer than the longitudinal one. In these experiments the appropriate Hurst exponent is calculated by fitting the (1d) SFM with the Ochs' formula [33]. In contrast, the EMU01 experiment on AB collisions [34] finds that the power law is valid for $H > 1.0$ *i.e.*, the longitudinal direction has to be partitioned finer than the transverse direction. An AB interaction is viewed as a superposition effect of many elementary NN interactions, as a result of which the effective Hurst exponent $H^{\text{eff}} \gg H$. On the other hand, in all of our experiments, previous and the present one, we consistently find that the power law of intermittency is obtained only if $H \neq 1$. It does not matter which direction (*i.e.*, longitudinal or transverse) is partitioned finer.

We have also calculated $F_q^{(2)}$ for $q = 2, 3$ and 4 using the optimized values of H obtained from $F_2^{(2)}$ analysis. Fig. 3 represents such plots, where $\ln F_q^{(2)}$ is plotted against $\ln M$, (a) for $H = 0.5$ and (b) for $H = 2.5$. The solid curves in either plot represent the linear fit to the data points, leaving first two points in each case for the same reason as mentioned earlier. The intermittency index $\phi_q^{(2)}$ is nothing but the slope of these linear fits, which indirectly is related with the intermittency strength. Table III shows the values of $\phi_q^{(2)}$ along with the χ^2(d.o.f.). One can see that the $\phi_q^{(2)}$ indices

obtained for a symmetric partitioning are much larger than the corresponding values for $H = 0.5$ and 2.5. Moreover, the $H = 0.5$ scaling reproduces larger $\phi_q^{(2)}$ than what we obtain for $H = 2.5$. Comparing with our previous works we find that the present set of self-affine $\phi_2^{(2)}$ values are of the same order of magnitude as those obtained in ^{32}S–Ag/Br and ^{16}O–Ag/Br interactions at 200A GeV [23].

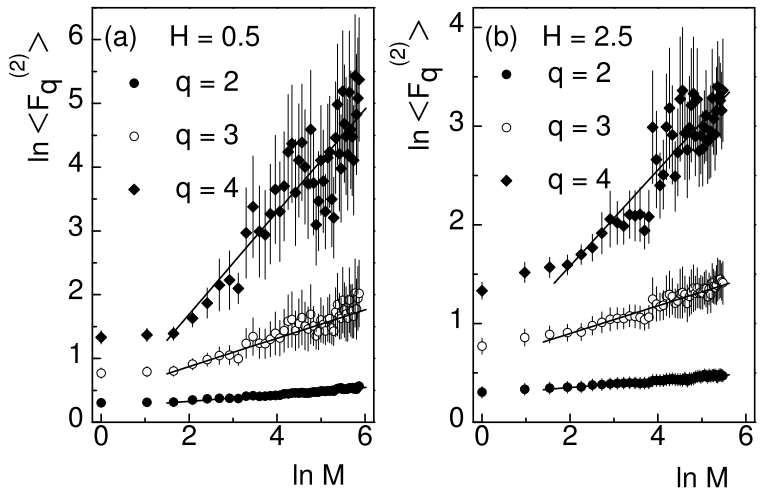

Fig. 3. Plot of $\ln\langle F_q^{(2)}\rangle$ *versus* $\ln M$ for $q = 2, 3$ and 4 for (a) $H = 0.5$ and (b) for $H = 2.5$. The lines represent linear regression leaving the first two points.

TABLE III

The (2d) intermittency exponents $\phi_q^{(2)}$ of the order of $q = 2,\ 3$ and 4 for unequal partitioning of η and φ directions.

Order	$H = 0.5$		$H = 2.5$	
	$\phi_q^{(2)}$	χ^2(d.o.f.)	$\phi_q^{(2)}$	χ^2(d.o.f.)
$q = 2$	0.053±0.004	06.39(46)	0.035±0.004	04.27(46)
$q = 3$	0.222±0.012	27.06(46)	0.141±0.008	16.82(46)
$q = 4$	0.778±0.033	46.23(46)	0.436±0.022	59.63(46)

A direct measure of the intermittency strength, in terms of the intermittency exponents, can be made in the framework of a random cascading model like the α-model [35]. According to this model, the strength parameter α_q is defined as

$$\alpha_q = \sqrt{\frac{6\ln 2}{q}(D - D_q)}\,. \tag{8}$$

where D_q is the qth order generalized Rényi dimension and D is the topological dimension (here 2) of the phase-space. In Fig. 4 (a) the α_q values are plotted against the order number q for both the H values. It can be seen that the strength parameter almost linearly increases with increasing order, though the values obtained for $H = 0.5$ are consistently greater than those for $H = 2.5$. In view of our observation mentioned above regarding the intermittency index, it is not surprising that the (2d) intermittency strength in ^{28}Si–Ag/Br interaction is of the same order of magnitude as those obtained in the ^{32}S–Ag/Br and ^{16}O–Ag/Br interactions at 200A GeV [23].

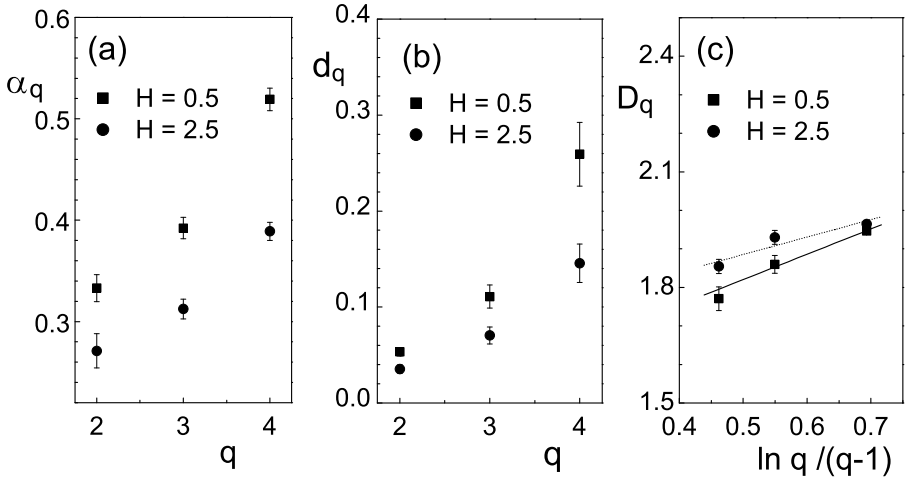

Fig. 4. Plots of (a) the intermittency strength α_q, (b) the anomalous fractal dimension d_q and (c) D_q *versus* $\ln q/(q-1)$. All points are for $H = 0.5$ and 2.5. The best linear fits are shown in (c).

The generalized dimension of (multi)fractality D_q is related to the anomalous fractal dimension d_q by [36]

$$D_q = D - d_q \,, \tag{9}$$

where d_q can be expressed in terms of the intermittency exponents as

$$d_q = \frac{\phi_q}{q-1} \,. \tag{10}$$

The direct relationship between intermittency and (multi)fractality is not yet fully understood. But it has been argued that, if a second-order phase transition from QGP to hadron phase takes place, then particle density distribution would show intermittency with an anomalous dimension d_q that

is independent of q [37]. On the other hand, hadronization through a cascading process will lead to d_q linearly increasing with q. The dependence of d_q on q is shown in Fig. 4 (b) for $H = 0.5$ and 2.5. The plot shows that the anomalous fractal dimension increases approximately linearly with increasing order q in both cases and the rate of increase for $H = 0.5$ is greater than that is for $H = 2.5$. Hence the observation is in agreement with the prediction of the cascade model.

A thermodynamic interpretation of multifractality has been given in terms of a constant specific heat C, provided the transition from monofractal to multifractal is governed by a Bernoulli type of fluctuation. Bershadski proposed a phenomenological relation among the generalized Rényi dimension D_q and C as [38]

$$D_q = D_\infty + \frac{C \ln q}{q-1}\,. \tag{11}$$

$C = 0$ in monofractal phase which becomes nonzero finite in the multifractal phase. In Fig. 4 (c) we have given a plot of D_q with $\ln q/(q-1)$. The multifractal specific heat is extracted by fitting straight line to the data points, as shown in the figure. For $H = 0.5$, $C = 0.657 \pm 0.083$; whereas, for $H = 2.5$, $C = 0.453 \pm 0.064$. This is for the first time that the multifractal specific heat is obtained in (2d). The present set of values are larger than the universal value $C(= 1/4)$ quoted in [38], are larger than the (1d) values of C in ^{32}S–Ag/Br and ^{16}O–Ag/Br interactions at 200A GeV [22], and they are very close to the (1d) values obtained in a similar ^{28}Si induced experiment [39].

5. Conclusion

We have performed a two-dimensional intermittency analysis of the shower track angular emission data of ^{24}Si–Ag/Br interaction at the incident energy 14.5A GeV. The following observations can be made from our analysis.

- The two-dimensional intermittency is much (several times) stronger than the one-dimensional intermittency of the same data set. Like in the one-dimensional case, due to the absence of any correlation between particles in the input, the UrQMD model alone cannot produce significant intermittency. When we numerically model the Bose–Einstein correlation and implement the same into the UrQMD output data, we find that there is a definite improvement as seen from the power law increase of the (2d) SFM. The experimental slope values are still several times larger than the simulation (UrQMD+BEC), and the upward bending that is so typical of the anisotropy in two-dimensional density distribution, is absent in the simulated (UrQMD+BEC) plot. Hence, we conclude that even by accommodating the Bose–Einstein

correlation at the after-burner level, one cannot fully reproduce the experimental observation. However, we would like to mention that the Bose–Einstein correlation has been accommodated into the UrQMD data as an after burner without any check on the two-particle correlations, and not directly at the correlation level. Hence, this method [19, 20] cannot be considered as a fully convincing way of taking into account the Bose–Einstein correlation effect as a probable cause of the intermittency in the ^{28}Si–Ag/Br interaction under consideration.

- As reflected from the upward bending in the variation of the scaled factorial moments, there is a strong anisotropy in the (η, φ) phase-space. This anisotropy is taken care of by introducing the Hurst exponent, which in the present case comes out to be 0.5 and 2.5. With the above choice of H values we retrieve the anomalous scaling of the SFM, and obtain the actual intermittency strength. As the anomalous scaling is obtained both for $H < 1$ and $H > 1$, in our case it is not mandatory that one particular direction (*e.g.*, longitudinal η or transverse φ) has to be partitioned finer with respect to the other. This in a sense contradicts the observations of similar nucleus–nucleus experiments [34, 40], and an interpretation of nucleus–nucleus results in terms of the superposition of many elementary nucleon–nucleon collisions seems inadequate [41].

- Using the appropriate H values we have determined the intermittency strength, the generalized multifractal dimension, and the multifractal specific heat. The (2d) intermittency strength is of the same order of magnitude as obtained from similar nucleus–nucleus experiments at a much higher incident energy (200 GeV per nucleon). This, in a sense, indicates that the intermittency phenomenon in nucleus–nucleus experiments is less sensitive to the variation in collision energy. The general nature of the fractal parameters obtained above tells us that a multifractal structure is present in the underlying dynamical fluctuation of the particle density function, which probably is an outcome of a random cascading process of particle production.

As suggested in [41] it would perhaps be more prudent if we could perform the single event intermittency analysis in two dimension, and could obtain the bending parameter 'a' for each event. A distribution of the bending parameter could have allowed us to identify whether or not particles from individual events are coming out from identical thermodynamic state. However, due to the limited multiplicities in our event sample such an exercise could not be undertaken.

REFERENCES

[1] A. Bialas, R. Peschanski, *Nucl. Phys.* **B273**, 703 (1986).

[2] A. Bialas, R. Peschanski, *Nucl. Phys.* **B308**, 857 (1988).

[3] P. Carruthers *et al.*, *Phys. Lett.* **B222**, 487 (1989).

[4] M. Gyulassy, L. van Hove, in: *Multiparticle Dynamics*, Eds. A. Giovannini, W. Kittel, World Scientific, Singapore 1990.

[5] K. Kadiza, P. Seyboth, *Phys. Lett.* **B287**, 363 (1992).

[6] I.M. Dremin, *Pisma Zh. Eksp. Teor. Fiz.* **30**, 152 (1979).

[7] A.E. Glassgold, W. Heckrotte, K.M. Watson, *Ann. Phys.* **6**, 1 (1959).

[8] I.M. Dremin, *Sov. J. Nucl. Phys.* **30**, 726 (1981).

[9] W. Ochs, *Phys. Lett.* **B247**, 101 (1990).

[10] A. Bialas, K. Zalewski, *Phys. Lett.* **B238**, 413 (1990).

[11] L. van Hove, *Z. Phys.* **C21**, 93 (1983).

[12] E. Shuryak, *Phys. Lett.* **B423**, 9 (1988).

[13] E.A. De Wolf, I.M. Dremin, W. Kittel, *Phys. Rep.* **270**, 1 (1996).

[14] W. Kittel, E.A. De Wolf, *Soft Multihadron Dynamics*, World Scientific, Singapore 2005.

[15] W. Ochs, *Z. Phys.* **C50**, 339 (1991).

[16] W. Ochs, *Acta Phys. Pol. B* **22**, 203 (1991).

[17] P. Mali, A. Mukhopadhyay, G. Singh, *Can. J. Phys.* **89**, 649 (2011).

[18] S.A. Bass *et al.*, *Prog. Part. Nucl. Phys.* **41**, 255 (1998).

[19] O.V. Utyuzh, G. Wilk, Z. Wlodarczyk, *Phys. Lett.* **B522**, 273 (2001).

[20] O.V. Utyuzh, G. Wilk, Z. Wlodarczyk, invited talk delivered by G. Wilk at the International Conference 'New Trends in High-energy Physics (Experiment, Phenomenology, Theory)' Yalta, Crimea, Ukraine, September 10–17, 2005.

[21] M.K. Ghosh, A. Mukhopadhyay, G. Singh, *J. Phys. G* **34**, 177 (2007).

[22] M.K. Ghosh *et al.*, *Int. J. Mod. Phys.* **E19**, 2229 (2010).

[23] M.K. Ghosh *et al.*, *Nucl. Phys.* **A858**, 67 (2011).

[24] C.F. Powell, P.H. Fowler, D.H. Perkins, *The Study of Elementary Particles by Photographic Method*, Pergamon, Oxford 1959.

[25] W.H. Barkas, *Nuclear Research Emulsions Vol. I and II*, Academic Press, New York 1963.

[26] W.H. Press, S.A. Teukolsky, W.T. Vetterling, B.P. Flannery, *Numerical Recipes in FORTRAN 90*, Cambridge University Press, New York 1990.

[27] M. Bystersky, *Nucleonica Supplement* **49**, S37 (2004).

[28] A. Bialas, M. Gazdzicki, *Phys. Lett.* **B252**, 483 (1990).

[29] L. Van Hove, *Phys. Lett.* **B28**, 429 (1969); *Nucl. Phys.* **B9**, 331 (1969).

[30] L. Liu, Y. Zhang, Y. Wu, *Z. Phys.* **C69**, 323 (1996).

[31] N.M. Agababyan *et al.* [NA22 Collaboration], *Phys. Lett.* **B382**, 305 (1996).
[32] S. Wang, Z. Wang, C. Wu, *Phys. Lett.* **B410**, 323 (1997).
[33] W. Ochs, *Phys. Lett.* **B247**, 101 (1990).
[34] M.I. Adamovich *et al.* [EMU01 Collaboration], *Z. Phys.* **C76**, 659 (1997).
[35] L. Lianshou, F. Jinghua, W. Yuanfang, *Phys. Lett.* **B444**, 563 (1998).
[36] G. Paladin, A. Vulpiani, *Phys. Rep.* **156**, 147 (1987).
[37] W. Ochs, *Z. Phys.* **C50**, 339 (1991).
[38] A. Bershadski, *Phys. Rev.* **C59**, 364 (1999).
[39] M. Mohsin Khan *et al.*, *Acta Phys. Pol. B* **38**, 2653 (2007).
[40] M.M. Haq, S. Islam, R. Hasan, *J. Phys. G* **30**, 1959 (2004).
[41] L. Lianshou [EMU01 Collaboration], *Nucl. Phys. Proc. Suppl.* **B71**, 341 (1999).